Journal of Sound and Vibration (1999) **227**(4), 711–734
Article No. jsvi.1999.2391, available online at http://www.idealibrary.com on IDEAL®

VIBRATION CONTROL OF BENDING MODES OF PLATES USING ACTIVE CONSTRAINED LAYER DAMPING

C. H. PARK

Department of Mechanical Engineering, The Catholic University of America, Washington DC 20064, *U.S.A.*

AND

A. BAZ

Mechanical Engineering Department, University of Maryland, College Park, MD 20742, *U.S.A.*

(*Received* 20 *September* 1996, *and in final form* 3 *May* 1999)

The fundamentals of active vibration control of plates are investigated theoretically and experimentally, using active constrained layer damping (ACLD) treatments. Particular emphasis is placed on controlling of the first two bending modes of vibration of plates which are treated fully with ACLD treatments using proportional and derivative control laws. Finite element models are developed to describe the dynamics of the ACLD. A modified version of laminated plate theory, which is an extension of the layer-wise Kirchhoff deformation relationships for the actuator/sensor layers and the base plate layer is introduced. Also, the Mindlin–Reissner plate theory is adopted to express the shear deformation characteristics of the viscoelastic layer. The models are validated experimentally at various operating conditions. The results obtained indicate the potential of the ACLD treatments as very effective means for damping the structural vibrations as compared to the conventional PCLD.

1. INTRODUCTION

Passive surface treatments have been extensively utilized, as a simple and reliable means, for damping the vibration of plain and sandwiched plates. These surface treatments rely in their operation on the use of constrained viscoelastic damping layers which are bounded to the vibrating structures. Higher damping ratios can also be obtained, over a broad range of temperatures and frequencies, through the use of multi-damping. Such performance is achieved, however, at the expense of adding considerable weight to the vibrating plate. This poses serious limitation to their practical use for many applications where the weight is of critical importance. Recently, considerable emphasis has been placed on controlling the vibration of plates using various passive and active control strategies. Important among these strategies is the passive electro-mechanical surface damping (EMSD) approach [1]

0022-460X/99/440711 + 24 $30.00/0

and the active constrained layer damping (ACLD) treatment [2, 3]. In both strategies, the vibrating plate is treated with a viscoelastic damping layer which is constrained by a piezoelectric film. The piezofilm is utilized to generate additional damping through the use of shunting circuits tuned to the dominant resonant frequencies of the vibrating plate as in the EMSD approach, or through controlling the shear deformation of the viscoelastic treatment as in the ACLD approach. The damping mechanism is generated by only passive means in the EMSD approach, and by a combination of active and passive means in the ACLD approach. In this paper, the attractive attributes of the ACLD approach are utilized to control, theoretically and experimentally, multi-bending modes of vibration of plates treated fully with patches of the ACLD. The ACLD is envisioned to be an effective means for augmenting the simplicity of passive damping with the low weight and high efficiency of active controls to attain high damping characteristics over broad frequency bands.

2. THE CONCEPT OF ACTIVE CONSTRAINED LAYER DAMPING

The ACLD treatment consists of a conventional passive constrained layer damping which is augmented with efficient active control means to control the strain of the constraining layer, in response to the structural vibrations as shown in Figure 1. The viscoelastic damping layer is sandwiched between two piezoelectric layers. The three-layer composite ACLD when bonded to the vibrating plate acts as a SMART constraining layer damping treatment with built-in sensing and actuation capabilities. The sensing, as indicated by the sensor voltage V_S is provided by the piezoelectric layer which is directly bonded to the plate surface. The actuation is generated by the other piezoelectric layer which acts as an active constraining layer that is activated by the control voltage V_C. With appropriate strain control, through proper manipulation of V_S, the shear deformation of the viscoelastic damping layer can be increased, the energy dissipation mechanism can be enhanced and the structural vibration can be damped out.

Also, the ACLD provides a practical means for controlling the vibration of massive structures with the currently available piezoelectric actuators without the need for excessively large actuation voltages. This is due to the fact that the ACLD properly utilizes the piezoelectric actuator to control the shear in the soft viscoelastic core which is a task compatible with the low control authority capabilities of the currently available piezoelectric materials.

3. FINITE ELEMENT ANALYSIS OF PLATE/ACLD SYSTEM

3.1. OVERVIEW

A finite element model is developed to describe the dynamics and control of flexible plates treated fully with the ACLD treatment. The model simulates the interaction between the base plate, the piezoelectric sensor/actuator, the viscoelastic damping layer, and the control laws. The model accounts for the

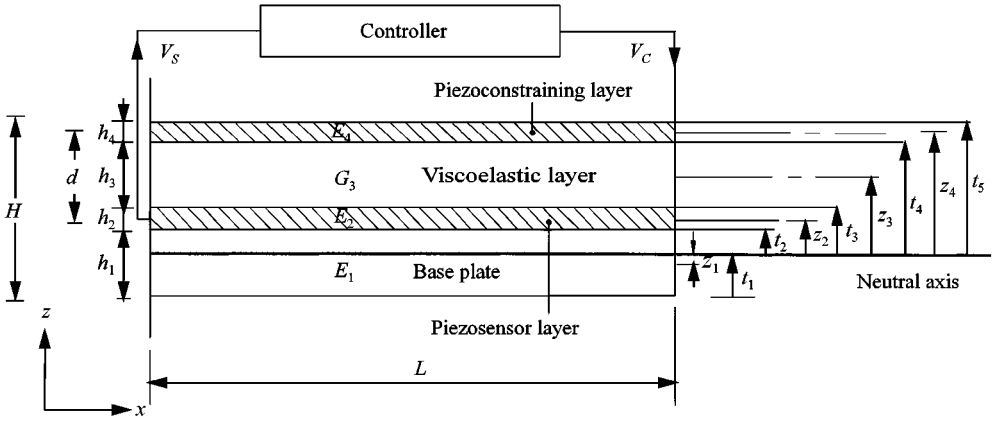

Figure 1. Schematic drawing of the plate/ACLD system.

behavior of the distributed piezoelectric sensor and actuator. The model utilizes quadrilateral finite elements each of which has four nodes with five degrees of freedom per node to describe the longitudinal displacements u_0 and v_0, the transverse deflection w, and the slopes $\partial w/\partial x$ and $\partial w/\partial y$ of the deflection line.

In this paper, a simple quadrilateral element is used to conform with the literature of passive constrained layer damping (PCLD) treatments, as for example in Khatua and Cheung [4]. The properties of the element are modified to account for the effect of the piezoelectric controller. Hence, when the piezocontrol action vanishes, the results converge to the conventional results of the PCLD which are familiar to the Passive Damping Community.

With reference to Figure 1, the plate has length L, thickness h_1, elastic modulus E_1 and density ρ_1. The sensor sheet has thickness h_2, Young's modulus E_2 and mass density ρ_2. The piezoelectric actuator has thickness h_4, Young's modulus E_4 and piezoelectric constant d_{31}. The viscoelastic layer has the thickness h_3, mass density ρ_3, complex shear modulus G_3 and Young's modulus E_3, $G_3 = G'(1 + i\eta_3)$ and $E_3 = E'(1 + i\eta_3)$, where the superscript $'$ indicates the elastic modulus and η_3 is the loss factor which is frequency and temperature dependent. In the sequel, subscripts 1 denote the base plate, 2 the sensor, 3 the viscoelastic and 4 the actuator.

The assumptions made in the following analysis are as follows: (1) A plane transverse to the middle plane before bending, remains plane and perpendicular to the middle plane after bending for the constraining, the sensor and the base plate layer. (2) The transverse displacement w at a section does not vary along thickness. (3) Displacement are small compared with the plate thickness. (4) The piezo-sensor/actuator layers and the base plate are assumed to be elastic and isotropic. (5) The viscoelastic layer is assumed to be linearly viscoelastic and characterized by a complex modulus $G_3 = G_3(1 + i\eta_3)$, where η_3 is the viscoelastic loss factor. (6) Perfect bonding between meeting surfaces is assumed.

3.2. MAIN PARAMETERS AND KINEMATIC RELATIONSHIPS

From the geometry of the ACLD system shown in Figure 1, the neutral axis can be determined by considering the force balance in the longitudinal direction x:

$$E_1 \int_{-t}^{-t+h_1} z\,\mathrm{d}z + E_2 \int_{-t+h_1}^{-t+h_1+h_2} z\,\mathrm{d}z + E_3 \int_{-t+h_1+h_2}^{-t+H-h_4} z\,\mathrm{d}z + E_4 \int_{-t+H-h_4}^{-t+H} z\,\mathrm{d}z = 0. \tag{1}$$

Equation (1) yields the expression

$$t_1 = (E_1h_1^2 + 2E_2h_1h_2 + E_2h_2^2 + 2E_3h_1h_3 + 2E_3h_2h_3 + E_3h_3^2 + 2E_4h_1h_4 + 2E_4h_2h_4 + 2E_4h_3h_4 + E_4h_4^2)/(2E_1h_1 + 2E_2h_2 + 2E_3h_3 + 2E_4h_4), \tag{2}$$

where t_1 is the distance between the bottom of the base plate and the composite neutral axis. Note also that

$$t_2 = h_1 + t_1, \qquad t_3 = h_2 + t_2, \qquad t_4 = h_3 + t_3, \qquad t_5 = h_4 + t_4, \tag{3}$$

$$z_1 = t_1 + h_1/2, \qquad z_2 = t_3 - h_2/2, \qquad z_3 = t_4 - h_3/2, \qquad z_4 = t_5 - h_4/2. \tag{4}$$

The shear strains γ_{xz} and γ_{yz} of the viscoelastic core can be written as [4]

$$\gamma_{xz} = d/h_3\,[(u_4 - u_2)/d - (w_{,x})],\ \gamma_{yz} = d/h_3\,[(v_4 - v_2)/d - (w_{,y})], \tag{5}$$

where $d = (h_3 + h_2/2 + h_4/2)$, with h_2, h_3, and h_4 denoting the thicknesses of the sensor, the viscoelastic core and actuator layer respectively. The subscripts $,x$ and $,y$ denote spatial derivatives with respect to x and y.

3.3. DEGREES OF FREEDOM AND SHAPE FUNCTIONS

The plate/ACLD elements considered are two-dimensional elements bounded by four nodal points as shown in Figure 2. The element has length a, width b and total thickness H. It is assumed that the origin of the Cartesian co-ordinates is at nodal point (1) and that there are five degrees of freedom for each nodal point. These degrees of freedom include the longitudinal displacements u_0 and v_0, transverse deflection w, slope in the x direction θ_x and slope in the y direction θ_y. It is assumed that the local element longitudinal displacements u, v are given in the following layer-wise displacements [5, 6] using the Kirchhoff deformation relationships for the actuator/sensor layers and the plate layer:

$$u_j = u_0 + z_j\theta_x, \qquad v_j = v_0 + z_j\theta_y, \qquad j = 1, 2, 4, \tag{6}$$

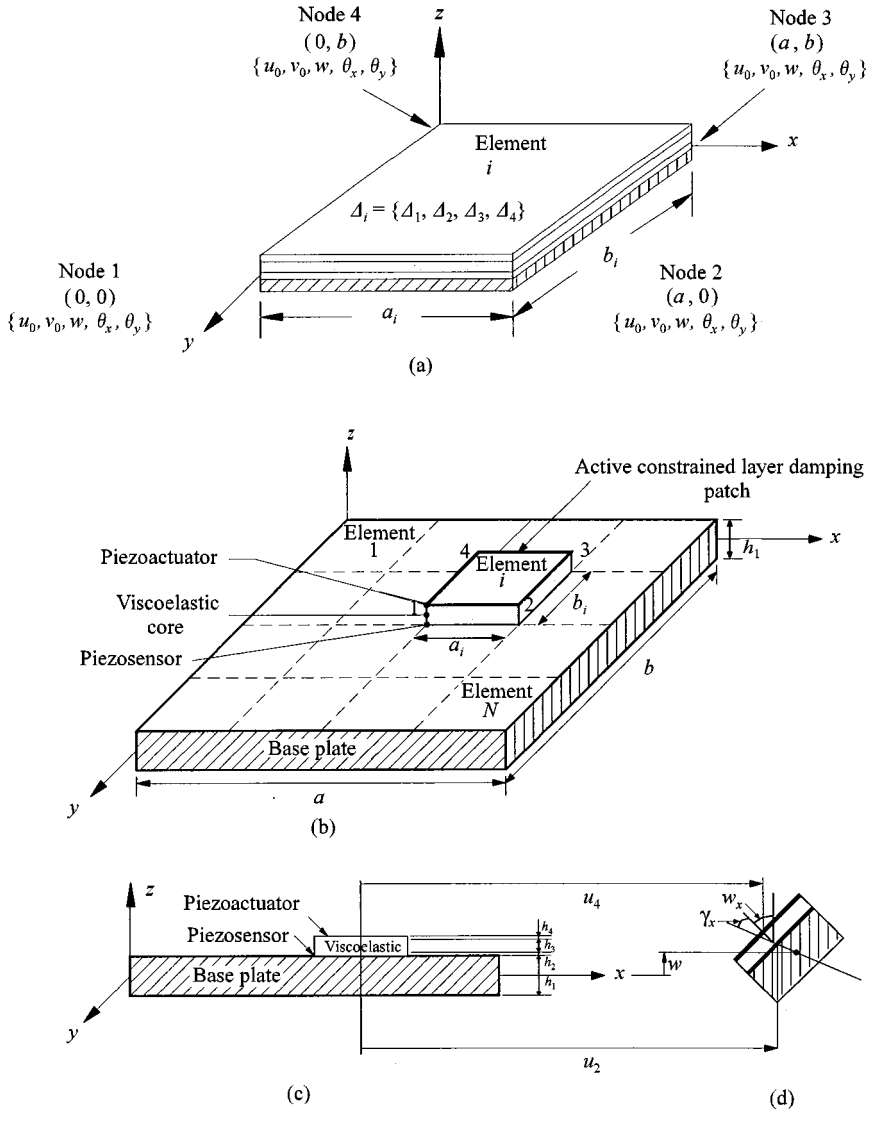

Figure 2. Finite element model of a plate treated with ACLD: (a) co-ordinate system, (b) main configuration, (c) undeflected plate cross-section, (d) deflected plate cross-section.

where $\theta_x = \partial w/\partial x$ and $\theta_y = -\partial w/\partial y$. The Mindlin–Reissner plate theory for the viscoelastic layer [7] gives

$$u_3 = u_0 + z_3\phi_x, \qquad v_3 = v_0 + z_3\phi_y, \qquad \phi_x = \gamma_{xz} + \theta_x, \qquad \phi_y = \gamma_{yz} + \theta_y, \quad (7)$$

where z_j is the z co-ordinate of the mid-plane of the jth layer measured from the neutral axis of the composite plate/ACLD; u_0 and v_0 are the in-plane longitudinal displacements of the neutral plane. ϕ_x and ϕ_y are the rotational variables for the viscoelastic core along x and y directions.

The spatial distributions of the longitudinal displacements, u_0 and v_0, and the transverse displacement w are given in the following form in terms of the local co-ordinates x and y:

$$u_0 = a_1 + a_2x + a_3y + a_4xy, \quad v_0 = a_5 + a_6x + a_7y + a_8xy, \tag{8, 9}$$

$$w = b_1 + b_2x + b_3y + b_4x^2 + b_5xy + b_6y^2 + b_7x^3 + b_8x^2y + b_9xy^2 + b_{10}y^3 + b_{11}x^3y + b_{12}xy^3. \tag{10}$$

The above equations can be combined and written in matrix form as

$$\{\Delta\} = \{u_0, v_0, w, \theta_x, \theta_y\}^{\mathrm{T}} = [X][a]. \tag{11}$$

The constants $\{a_1, a_2, \ldots, a_8\}$ and $(b_1, b_2, \ldots, b_{12})$ are determined in terms of the 20 components of the nodal deflection vector $\{\Delta_i\}$ of the ith element which is bounded by the nodes 1, 2, 3 and 4. From Figure 2, the nodal co-ordinates are

$$\text{Node1: } (0, 0), \quad \text{Node2: } (a, 0), \quad \text{Node3: } (a, b), \quad \text{Node4: } (0, b).$$

Substituting these nodal co-ordinate values into equation (11) and solving for $\{a\}$, the following equation is obtained:

$$\{\Delta_i\} = \{\Delta_1, \Delta_2, \Delta_3, \Delta_4\}^{\mathrm{T}} = [A]\{a\}, \tag{12}$$

where $\{\Delta_k\} = \{u_{0k}, v_{0k}, w_k, \theta_{x_k}, \theta_{y_k}\}^{\mathrm{T}}$ for $k = 1, \ldots, 4$. From equation (12), $\{a\}$ can be obtained, $\{a\} = [A]^{-1}\{\Delta_i\}$. Substituting $\{a\}$ into equation (11), the deflection $\{\Delta\}$ at any location (x, y) inside the ith element can be determined from

$$\{\Delta\} = \{u_0, v_0, w, \theta_x, \theta_y\}^{\mathrm{T}} = [\{N_1\}, \{N_2\}, \{N_3\}, \{N_4\}, \{N_5\}]^{\mathrm{T}}\{\Delta_i\} = [N]\{\Delta_i\}, \tag{13}$$

where $\{N_1\}$, $\{N_2\}$, $\{N_3\}$, $\{N_4\}$ and $\{N_5\}$ are the spatial interpolating vectors corresponding to u_0, v_0, w, θ_x and θ_y respectively. The in-plane displacements shape function of the each layer are obtained as

$$[N_j]_u = [N_1] + z_j[N_{3,x}], \qquad [N_j]_v = [N_2] + z_j[N_{3,y}], \tag{14}$$

where the subscript, j, represents the actuator/sensor and the base plate layer and $,x$ and $,y$ denote the spatial derivatives with respect to x and y. Using the strain–displacement relationships, the strain vector is obtained as

$$\{\varepsilon\} = [d]\{\Delta\} = [d][N]\{\Delta_i\} = [B]\{\Delta_i\}, \tag{15}$$

where $[d]$ is the linear differential operator of the classical plate theory.

3.4. EQUATION OF MOTION

Applying the principle of virtual work to a finite element of the plate/ACLD system yields

$$\delta\{\Delta_i\}^{\mathrm{T}}\iiint_V [B]^{\mathrm{T}}[E][B]\,\mathrm{d}V\{\Delta_i\} = \delta\{\Delta_i\}^{\mathrm{T}}\iiint_V [N]^{\mathrm{T}}\{b(x,y,t)\}\,\mathrm{d}V$$

$$+\,\delta\{\Delta_i\}^{\mathrm{T}}\iiint_V [N]^{\mathrm{T}}\{F\}\,\mathrm{d}V - \delta\{\Delta_i\}^{\mathrm{T}}\iiint_V \rho[N]^{\mathrm{T}}[N]\,\mathrm{d}V\{\ddot{\Delta}_i\}, \tag{16}$$

where $\delta\{\Delta_i\}$ is the virtual nodal deflection vector, $[E]$ is the rigidity operator matrix, $\{b(x, y, t)\}$ is the external body force vector and $\{F\}$ is the external force vector. Also, ρ and V denote the density and volume of element. Factoring out $\delta\{\Delta_i\}$, the stiffness matrix and the consistent mass matrix are defined as

$$[K] = \iiint_V [B]^{\mathrm{T}}[E][B]\,\mathrm{d}V, \quad [M] = \iiint_V \rho[N]^{\mathrm{T}}[N]\,\mathrm{d}V. \tag{17}$$

When ignoring the equivalent nodal loads due to the body force b, the dynamics of the ACLD-treated plate element can be described by the equation of motion,

$$[M_i]\{\ddot{\Delta}_i\} + [K_i]\{\Delta_i\} = \{F_c\}, \tag{18}$$

where $[K_i]$ and $[M_i]$ denote the stiffness and mass matrices of the plate/ACLD element which are described in detail in Appendix A. In equation (18). $\{F_c\}$ is the vector of control forces and moments generated by the piezoconstraining layer on the treated plate element. It is expressed as

$$\{F_c\} = \{F_1, F_2, F_3, F_4\}^{\mathrm{T}}, \qquad \{F_k\} = \{F_{pxk}, F_{pxk}, 0, M_{pxk}, M_{pxk}\}^{\mathrm{T}} \quad \text{for } k = 1, \ldots, 4, \tag{19, 20}$$

where F_{pxk}, F_{pyk}, M_{pxk} and M_{pyk} denote the control forces and moments generated at node k.

Equation (18) describes the dynamics/control of a single plate/ACLD element. Assembly of the corresponding equations for the different elements and applying the proper boundary conditions yields the overall equation for the entire plate/ACLD system.

3.5. PIEZOELECTRIC SENSOR

The voltage generated by the piezosensor due to plate vibration can be determined from the electric field displacement $\{D\}$ and the piezoelectric

constitutive equation,

$$q(t) = \iint_s D \, \mathrm{d}x \, \mathrm{d}y \tag{21}$$

with

$$\{D\} = [d]^{\mathrm{T}} \{T\} + [\varepsilon]^{\mathrm{T}} \{E\}, \tag{22}$$

where $q(t)$, $[d]$, $\{T\}$, $[\varepsilon]$ and $\{E\}$ represent the charge, piezoelectric strain constant, stress, dielectric permittivity and applied field strength matrix respectively [8]. When piezoelectric sensors are used as the strain rate sensors, the total charge can be transformed into an output voltage,

$$V_S(t) = \frac{1}{C} q(t), \tag{23}$$

where C is the capacitance of the distributed film sensor of specified dimensions given by

$$\mathrm{C} = 8{\cdot}854(10^{-12}) A k_{3t}/h_2, \tag{24}$$

where A is the sensor surface area and K_{3t} is the dielectric constant. The voltage V_S developed by the piezosensor can then be obtained as

$$V_S = \frac{1}{C} \sum_{i_{sx}}^{i_{fx}} \sum_{i_{sy}}^{i_{fy}} \int_{ai} \int_{bi} \left\{ \Lambda(x, y) [d_{3i}]^{\mathrm{T}} [Q_{ij}] \begin{bmatrix} u_{2,x} - z_2 w_{,xx} \\ v_{2,y} - z_2 w_{,yy} \\ u_{2,y} + v_{2,x} - 2 z_2 w_{,xy} \end{bmatrix} \right\} \mathrm{d}x \, \mathrm{d}y \tag{25}$$

or

$$V_S = [B_S] \{\Delta_i\}, \tag{26}$$

where

$$[B_S] = \frac{1}{C} \sum_{i_{sx}}^{i_{fx}} \sum_{i_{sy}}^{i_{fy}} \int_{ai} \int_{bi} \left\{ \Lambda(x, y) [d_{3i}]^{\mathrm{T}} [Q_{ij}] \left\{ \begin{bmatrix} [N_{1,2}]_{,x} \\ [N_{2,2}]_{,y} \\ [N_{1,2}]_{,y} + [N_{2,2}]_{,x} \end{bmatrix} - z_2 \begin{bmatrix} [N_3]_{,xx} \\ [N_3]_{,yy} \\ 2[N_3]_{,xy} \end{bmatrix} \right\} \right\} \mathrm{d}x \, \mathrm{d}y \tag{27}$$

and where $\Lambda(x, y)$ is a distribution shape function of the sensor [$\Lambda(x, y) = 1$ for uniform sensor], $[Q_{ij}]$ is the plane stress-reduced rigidity matrix. In equation (25), the sensor is extended between elements i_{sx} and i_{fx} in the x direction and i_{sy} and i_{fy} in the y direction.

The actuator voltage V_C is generated by applying a proportional and derivative control law to the piezosensor voltage V_S

$$V_C = -k_p V_S - k_d(\mathrm{d}V_S/\mathrm{d}t), \tag{28}$$

where k_p and k_d are the proportional and derivative control gains respectively.

3.6. CONTROL FORCES AND MOMENTS GENERATED BY PIEZOACTUATOR

The control forces and moments generated by the control voltage V_C are developed using the approach of reference [9]. First, consider the work done W_{P_F} by the in-plane piezoelectric forces $\{F_{pk}\}$ which can be expressed as

$$W_{P_F} = \{\Delta_k\}^{\mathrm{T}} \begin{Bmatrix} F_{pk} \\ 0 \\ 0 \\ 0 \end{Bmatrix} = h_4 \int_{ai}\int_{bi} \{\sigma_{4p}\}^{\mathrm{T}} \{\varepsilon_c\}\, \mathrm{d}x\, \mathrm{d}y, \tag{29}$$

where $\{\sigma_{4p}\}$ and $\{\varepsilon_c\}$ are the in-plane stress and strain vectors induced by the piezoelectric actuator layer 4, and

$$\begin{Bmatrix} F_{pk} \\ 0 \end{Bmatrix} = \begin{Bmatrix} F_{pxk} \\ F_{pyk} \\ 0 \end{Bmatrix} = (k_p + k_d\, \mathrm{d}/\mathrm{d}t)\, V_S \int_{ai}\int_{bi} \left\{ [B_{4p}]^{\mathrm{T}} [D_{4p}] \begin{bmatrix} d_{31} \\ d_{32} \\ 0 \end{bmatrix} \right\} \mathrm{d}x\, \mathrm{d}y, \tag{30}$$

where node $k = 1, \ldots, 4$. The constants d_{31} and d_{32} define the piezoelectric strain constants in the x and y directions.

Similarly, the work done W_{P_M} by the piezoelectric moments $\{M_{pk}\}$ due to the bending of the piezoelectric constraining layer can be obtained using the same procedure:

$$W_{P_M} = \{\Delta_k\}^{\mathrm{T}} \begin{Bmatrix} 0 \\ 0 \\ 0 \\ M_{pk} \end{Bmatrix} = h_4 \int_{ai}\int_{bi} \{\sigma_{4b}\}^{\mathrm{T}} \{\varepsilon_b\}\, \mathrm{d}x\, \mathrm{d}y, \tag{31}$$

where $\{\sigma_{4b}\}$ and $\{\varepsilon_b\}$ are the bending stress and strain vectors induced by the piezoelectric actuator layer 4, and

$$\begin{Bmatrix} M_{pk} \\ 0 \end{Bmatrix} = \begin{Bmatrix} M_{pxk} \\ M_{pyk} \\ 0 \end{Bmatrix} = (k_p + k_d \, \mathrm{d}/\mathrm{d}t) \, V_S \int_{ai} \int_{bi} z_4 \left\{ [B_b]^{\mathrm{T}} [D_{4b}] \begin{bmatrix} d_{31} \\ d_{32} \\ 0 \end{bmatrix} \right\} \mathrm{d}x \, \mathrm{d}y, \quad (32)$$

where $[D_{4b}]$ are defined as

$$[D_{4b}] = \begin{bmatrix} D_{4b11} & D_{4b12} & 0 \\ D_{4b21} & D_{4b22} & 0 \\ 0 & 0 & D_{4b33} \end{bmatrix} \quad (33)$$

with $D_{4b11} = D_{4b22} = E_4 I_4/(1 - v_4^2)$, $D_{4b12} = D_{4b21} = v_4 D_{4b11}$ and $D_{4b33} = D_{4b11}(1 - v_4)/2$, where I_4 denotes the area moment of inertia of the active constraining layer. These factors and moments depend on the capacitance C of the distributed film sensor, control gains and properties of the piezosensor and actuator.

The finite element model as described by equation (18) coupled with the piezosensor equations (25) and (26) and the piezoactuator equations (19), (20), (30) and (32) are used to predict the eigenvalues of the open-loop and closed-loop plate/ACLD system at different operating conditions. The eigenvalues being complex yield the natural frequencies and loss factors of the entire assembly.

4. EXPERIMENTAL IMPLEMENTATION OF PLATE/ACLD SYSTEM

4.1. OVERVIEW

The theoretical predictions of the ACLD model are compared with the experimental performance of an aluminium plate which is treated with a viscoelastic layer (DYAD-606 from Soundcoat, Deer Park, NY) sandwiched between treated two layers of PolyVinyliDene Fluoride (PVDF) piezoelectric films (AMP, Valley Forge, PA). In this regard, a plate with full ACLD treatment is tested at different control gains while operating at various ambient temperatures (25, 35 and 45°C). Hence, the effect of proportional and derivative control action on the system performance is presented. The experimental work in this section aims also at demonstrating the merits of the ACLD as an effective means for suppressing the vibration of the flat plates.

4.2. MATERIAL PROPERTIES

Tables 1 and 2 list the main physical and geometrical parameters of the aluminum sheet, DYAD-606 and polymeric films (Model number S028NAO).

TABLE 1
Physical and geometrical properties of the plate, viscoelastic and PVDF layer

Layer	Thickness (m)	Young's modulus (Pa)	Density (kg/m^3)	The Poisson ratio
ALUMINUM	4·064E-4	7·1E10	2700	0·33
DYAD-606	5·08E-5	*	1105	0.49
PVDF	2·8E-5	2·5E9	1780	0·3

* Depending on temperature and frequency.

TABLE 2
Main piezoelectric parameters of the PVDF film (at room temperature)

d_{31} (m/V)	d_{32} (m/V)	k_{31} (%)	k_{32} (%)	k_{3t}	g_{31} (Vm/N)	g_{32} (Vm/N)
23E-12	3E-12	12	10	12	216E-3	19E-3

Figure 3 shows the effect of the frequency (1–1000 Hz) and temperatures (25, 35 and 45°C) on the storage shear modulus G' of the DYAD-606. The important effect of frequency is that the shear moduli at different temperatures always increase with increasing frequency. Also, the shear modulus decreases with increasing temperature. As far as the loss factor is concerned, it can be seen in Figure 3(b) that it increases to a maximum and then decreases with increasing frequency when the temperature is 25°C. The position of maximum shifts to higher frequencies with increasing temperature. These curves are used to predict the performance of the ACLD treatment at different operating temperatures and frequencies.

4.3. EXPERIMENTAL SET-UP AND PROCEDURES

Figure 4 shows a photograph of the experimental set-up used in testing the effectiveness of the Active Constrained Layer Damping in attenuating the vibration of the test plate as compared with conventional passive constrained layer damping. The plate/ACLD system which is 25·4 cm long and 12·7 cm wide is mounted in a cantilevered configuration inside a temperature-controlled chamber (Model 5900, Delta Design, Inc.). A uniformly distributed piezoactuator is used to control the first two bending modes of the plate/ACLD system.

Figure 5 shows a schematic drawing of the set-up indicating that the internal function generator of the spectrum analyzer (Model CF910, ONO SOKKI) is used to generate a sine-wave sweep linearly from 0 to 35 Hz with a sweep rate 0·025 Hz/s. This sine wave is used to acoustically excite the plate/ACLD system through a loud speaker powered by power amplifier (Model 6260, Urel Electronic Co.). The tip

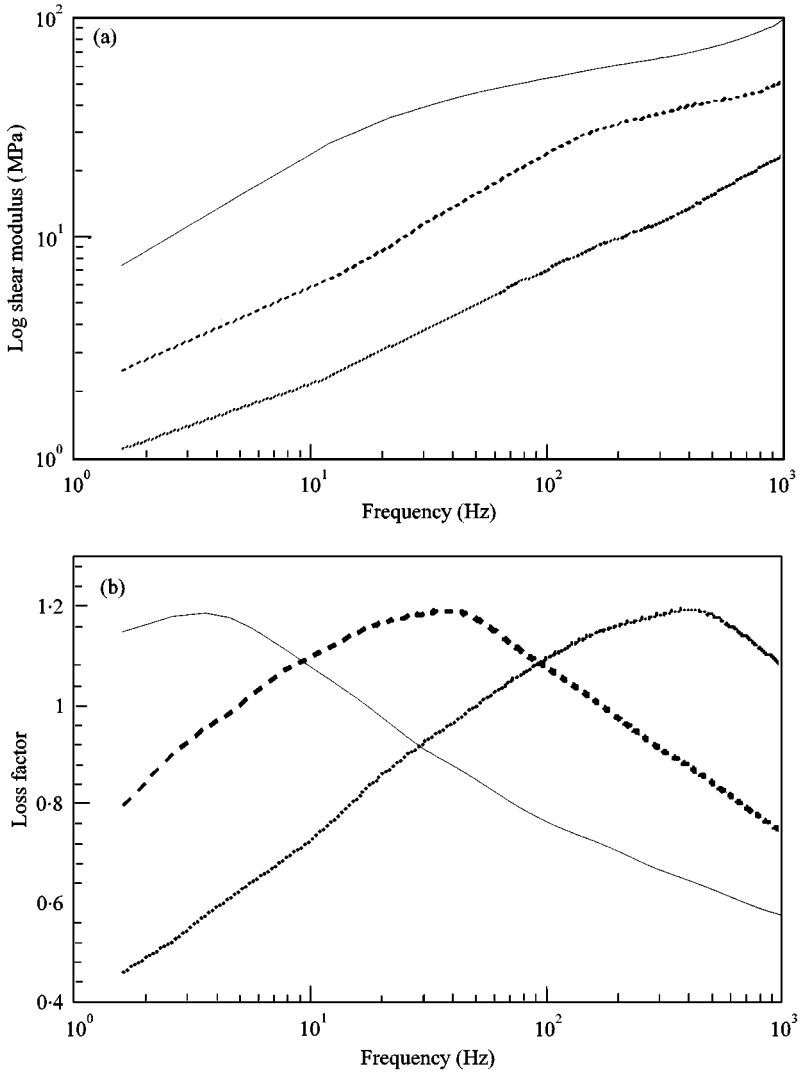

Figure 3. Frequency dependence of (a) shear modulus and (b) loss factor for DYAD-606. Temperatures: —, 25°C; - - -, 35°C; · · ·, 45°C.

displacement signal is measured by laser sensor (Model MQ-Aeromat Corp., Providence, NJ) at the middle-end of the test plate and is fed to the spectrum analyzer to determine its frequency content. The laser sensor has an accuracy of 20 μm over a frequency band between 0 and 1000 Hz. The magnitude ratio (dB) and the phase shift (deg) of the system response are automatically displayed and stored in the analyzer. Thus, the transfer function between the input and output can be obtained. Figure 5 also shows that another spectrum analyzer (Model CF-350, ONO SOKKI) is independently used to obtain the transfer function between the piezoactuator and piezosensor. The signal from the piezoelectric sensor is amplified using a charge amplifier (Model AM-5, Wilcoxon Research, Rockville, MD). An

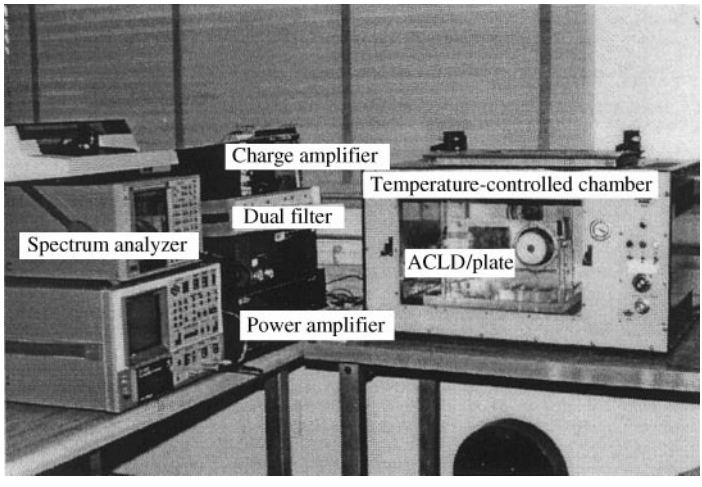

Figure 4. Experimental set-up for plate/ACLD system.

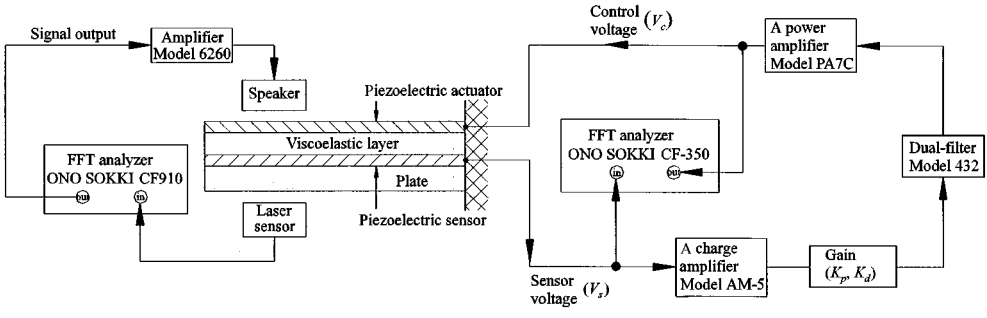

Figure 5. Schematic drawing of the experimental set-up.

analog circuit is used to generate a proportional and derivative control law. An analog filter (Model 432, Waveteck Co.) is then used to filter out the high-frequency content to avoid observation spillover. The resulting control action is sent via an analog power amplifier (Model PA7C, Wilcoxon Research) to the piezoelectric actuator layer and the spectrum analyzer to determine the frequency content and the amplitude of vibration.

4.4. EXPERIMENTAL RESULTS AT DIFFERENT OPERATING TEMPERATURES

The experimental results are presented at three different temperatures (25, 35 and 45°C). Comparisons are shown in this section between the amplitudes of vibration when the ACLD is unactivated (i.e., it acts as a Conventional Passive Constrained Layer Damping—PCLD) and when it is activated using three different proportional control gains at a fixed temperature.

A comparison between the natural frequencies, loss factors and attenuations of the untreated plain plate and plate treated with the PCLD (with $k_p = 0$ and $k_d = 0$) at temperature 25°C is shown in Tables 3 and 4. It is evident that the PCLD treatment has been very effective in attenuating the structural vibration of the plate over the considered frequency range. Tables 5–10 show that activating the ACLD treatment has resulted in effective attenuation of the plate vibrations at different operating temperatures. Also, it is evident that increasing the control gain has resulted in improving the vibration attenuation characteristics of the plate with the ACLD treatment. The performance is obtained using different proportional and derivative control gains ($k_p = 30$ with $k_d = 50$, $k_p = 60$ with $k_d = 130$ and $k_p = 120$ with $k_d = 220$). The maximum attenuations obtained are 81·4, 81·1 and 83·9% for

TABLE 3

The natural frequencies, loss factors and attenuations of the first bending mode for plain plate and PCLD at temperature 25°C

T:25°C	First bending mode Frequency	Loss factor	Attenuation (%)
Plate	4·72	0·034	
PCLD	4·48	0·042	62·86

TABLE 4

The natural frequencies, loss factors and attenuations of the second bending mode for plain plate and PCLD at temperature 25°C

T:25°C	Second bending mode Frequency	Loss factor	Attenuation (%)
Plate	30·375	0·012	
PCLD	27·58	0·035	83·01

TABLE 5

The natural frequencies, loss factors and attenuations of the first bending mode for full ACLD treatment at temperature 25°C

T:25°C k_p, k_d	First bending mode Frequency	Loss factor	Attenuation (%)
$k_p = 00$, $k_d = 00$	4·48	0·042	
$k_p = 30$, $k_d = 50$	4·65	0·075	44·4
$k_p = 60$, $k_d = 130$	4·75	0·147	75·3
$k_p = 120$, $k_d = 220$	4·94	0·182	81·4

TABLE 6
The natural frequencies, loss factors and attenuations of the second bending mode for full ACLD treatment at temperature 25°C

T:25°C k_p, k_d	Second bending mode Frequency	Loss factor	Attenuation (%)
$k_p = 00$, $k_d = 00$	27·58	0·035	
$k_p = 30$, $k_d = 50$	27·80	0·046	11·9
$k_p = 60$, $k_d = 130$	28·00	0·060	30·2
$k_p = 120$, $k_d = 220$	27·96	0·133	57·7

TABLE 7
The natural frequencies, loss factors and attenuations of the first bending mode for full ACLD treatment at temperature 35°C

T:35°C k_p, k_d	First bending mode Frequency	Loss factor	Attenuation (%)
$k_p = 00$, $k_d = 00$	4·40	0·048	
$k_p = 30$, $k_d = 50$	4·48	0·067	49·8
$k_p = 60$, $k_d = 130$	4·53	0·147	76·5
$k_p = 120$, $k_d = 220$	4·64	0·187	81·1

TABLE 8
The natural frequencies, loss factors and attenuations of the second bending mode for full ACLD treatment at temperature 35°C

T:35°C k_p, k_d	Second bending mode Frequency	Loss factor	Attenuation (%)
$k_p = 00$, $k_d = 00$	26·19	0·030	
$k_p = 30$, $k_d = 50$	26·20	0·035	20·82
$k_p = 60$, $k_d = 130$	26·29	0·046	45·19
$k_p = 120$, $k_d = 220$	26·38	0·056	55·70

TABLE 9
The natural frequencies, loss factors and attenuations of the first bending mode for full ACLD treatment at temperature 45°C

T:45°C k_p, k_d	First bending mode Frequency	Loss factor	Attenuation (%)
$k_p = 00$, $k_d = 00$	4·30	0·042	
$k_p = 30$, $k_d = 50$	4·24	0·068	55·0
$k_p = 60$, $k_d = 130$	4·32	0·133	77·8
$k_p = 120$, $k_d = 220$	4·34	0·184	83·9

TABLE 10
The natural frequencies, loss factors and attenuations of the second bending mode for full ACLD treatment at temperature 45°C

T:45°C k_p, k_d	Second bending mode Frequency	Loss factor	Attenuation (%)
$k_p = 00$, $k_d = 00$	25·30	0·026	
$k_p = 30$, $k_d = 50$	25·72	0·036	14·6
$k_p = 60$, $k_d = 130$	26·31	0·044	40·5
$k_p = 120$, $k_d = 220$	26·40	0·052	49·7

the first bending mode and 57·7, 55·7 and 49·7% for the second bending mode when the operating temperature is set at 25, 35 and 45°C respectively. At 25°C, the vibration suppression for the full ACLD treatment is found to be most effective as compared to the other temperatures. It is also found that the closed-loop frequencies and loss factors, at the three temperatures, increase with increasing the control gains. However, the closed-loop frequencies are found to decrease with increasing operating temperature. Figure 6 summarizes that the ACLD strategy with control gains is very effective in attenuating the structural vibration of the plate at its first two bending modes.

The performances of a plain plate, plate/PCLD and plate/ACLD system, at control gains $k_\rho = 120$ with $k_d = 220$, are compared at different operating temperatures (25, 35 and 45°C). Figure 7 indicates that the PCLD strategy is very effective in attenuating the structural vibration of the plain plate. However, these attenuations are much lower than those obtained with the ACLD at the three different temperatures. Hence, it is concluded that the ACLD treatment is superior to the PCLD treatment particularly over wide temperature and frequency ranges. Such superiority stems from its ability to combine the attractive attributes of both the passive and active controls to produce lower amplitudes of vibration.

It is important to note that the control of the first and second bending modes which occur at 4·48 and 27·58 Hz did not result in control spillover or excitation of the first torsion mode of the plate which occurs at 14·5 Hz. This feature is displayed clearly in Figures 6 and 7.

4.5. COMPARISON BETWEEN THEORETICAL AND EXPERIMENTAL MODAL PARAMETERS

The finite element model is used to predict the theoretical natural frequencies and loss factors of the plate/PCLD and plate/ACLD systems. In this study, the plate/ACLD system is divided into 25 elements. The characteristic eigenvalue equations of the plate/ACLD are obtained after assembling the corresponding stiffness and mass matrices of elements which is derived in Appendix A. The

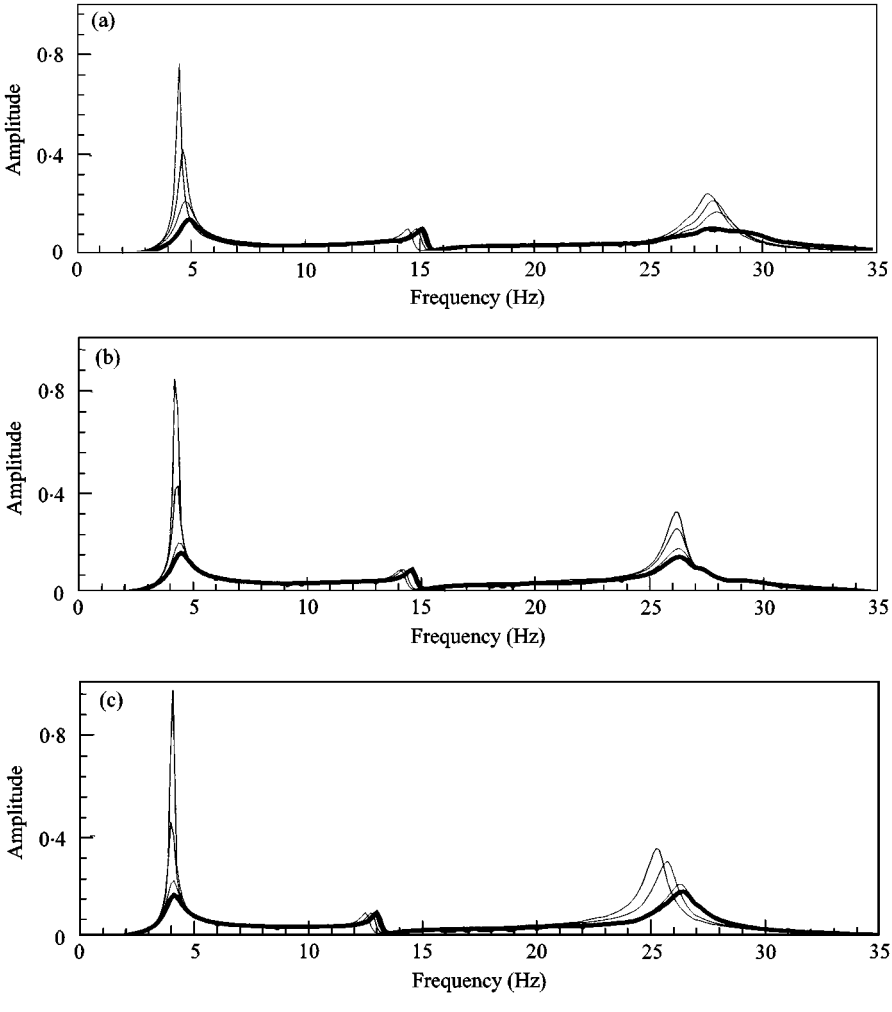

Figure 6. The frequency response of normalized attenuation of vibration amplitude for full ACLD treatment: (a) 25°C, (b) 35°C, (c) 45°C, controlled by k_p and k_d: —, $k_p = 00$, $k_d = 00$; —, $k_p = 30$, $k_d = 50$; —, $k_p = 60$, $k_d = 130$; —, $k_p = 120$, $k_d = 220$.

resulting equations are

$$\{[K] - \omega^{*2}[M]\}\{\Phi\} = 0, \tag{34}$$

where ω^* is the system frequency (rad/s) and $\{\Phi\}$ is the corresponding eigenvector. The eigenvalues in equation (34) are solved using the IMSL complex variables subroutines. This yields complex eigenvalues which are expressed as

$$\omega^{*2} = \omega^2(1 + i\eta), \tag{35}$$

where η is the loss factor of the system corresponding to the modal frequency ω.

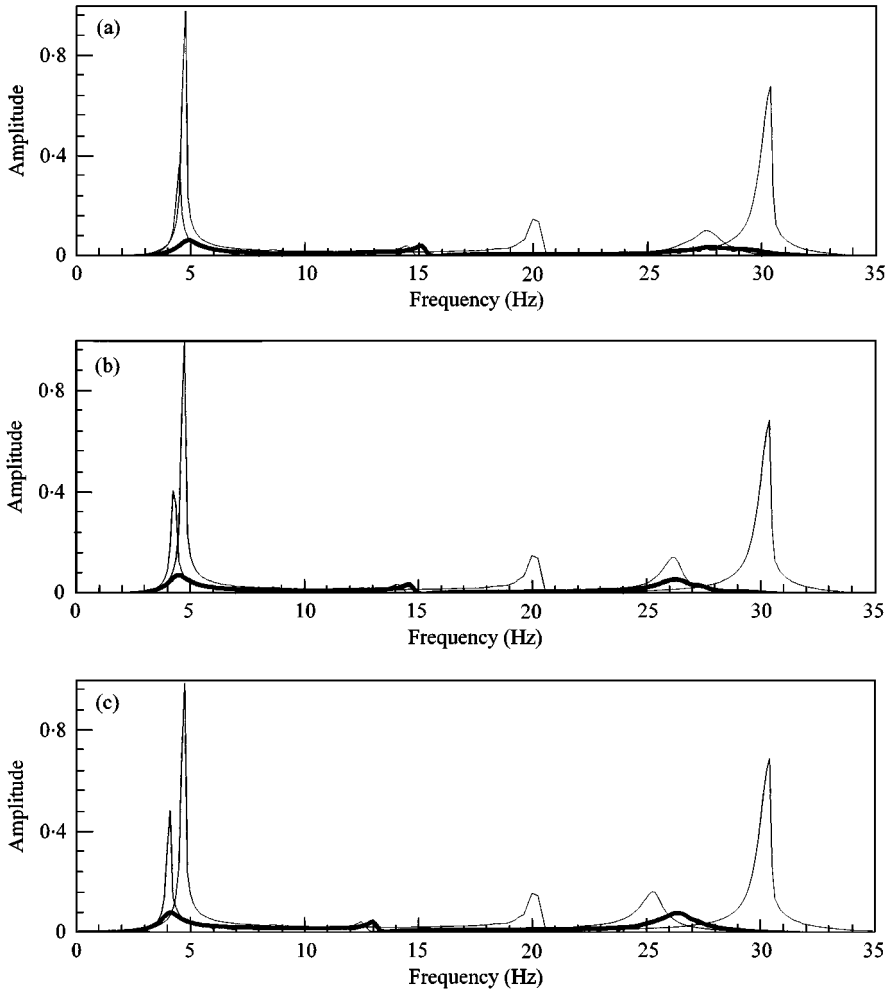

Figure 7. The frequency response of normalized attenuation of vibration amplitude for plain plate (—), plate/PCLD (—), plate/ACLD (—: optimum gain); (a) 25°C, (b) 35°C, (c) 45°C.

The theoretical and experimental modal frequencies and associated loss factors are compared for the first two bending modes when the full ACLD treatment is controlled with different proportional and derivative control gains at different operating temperatures (25, 35 and 45°C). Figures 8–11 summarize these results for different control gains. Figures 8 and 9 show comparisons between theoretical and experimental natural frequencies and loss factors of the first bending mode for the full ACLD treatment system at three different temperatures (25, 35 and 45°C). The results show a good agreement between theory and experiment. The discrepancy is about 3–6% in the modal frequencies and about 4–7% in the modal damping ratios respectively. Figures 10 and 11 show the corresponding comparisons between theoretical and experimental natural frequencies and loss factors of the second bending mode for the full ACLD treatment system at three different operating

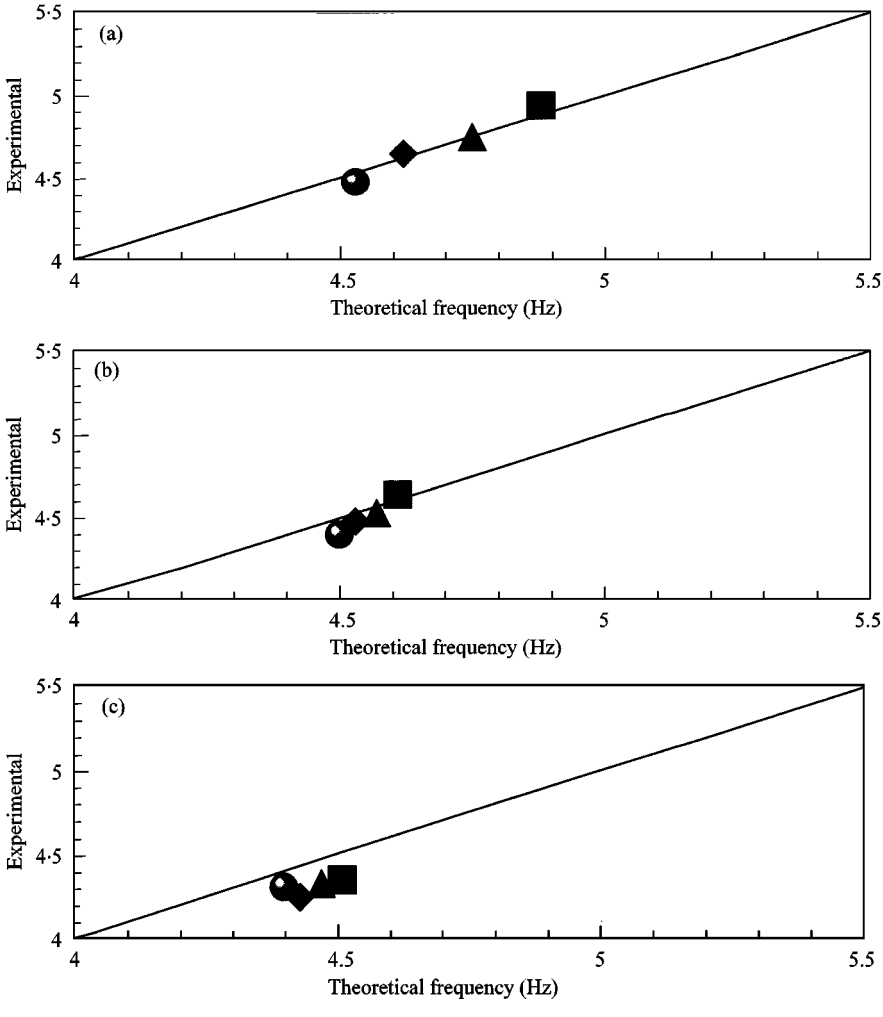

Figure 8. Comparison between theoretical and experimental natural frequencies of first bending mode for different k_p and k_d at (a) 25°C, (b) 35°C, (c) 45°C for full ACLD treatment (●, $k_p = 00$, $k_d = 00$; ◆, $k_p = 30$, $k_d = 50$; ▲, $k_p = 60$, $k_d = 130$; ■, $k_p = 120$, $k_d = 220$).

temperatures (25, 35 and 45°C). Close agreement between theoretical predictions and experimental measurements is evident. In addition, it is clear that the closed-loop frequencies decrease with increasing operating temperature, since the shear modulus of viscoelastic material decreases with increasing temperature as indicated in Figure 3. It is concluded that the results for the modal parameters estimated theoretically correlate well with the results from the experiments.

It is important here to note that the theoretical predictions presented are obtained using a finite element model with 25 elements. The convergence of the model is checked using 2, 8, 16 and 25 elements. With two elements, the first and second bending natural frequencies are 5·46 and 34·77 Hz, with eight elements, the values become 4·53 and 28·51 and with 16 elements, the frequencies are 4·52 and

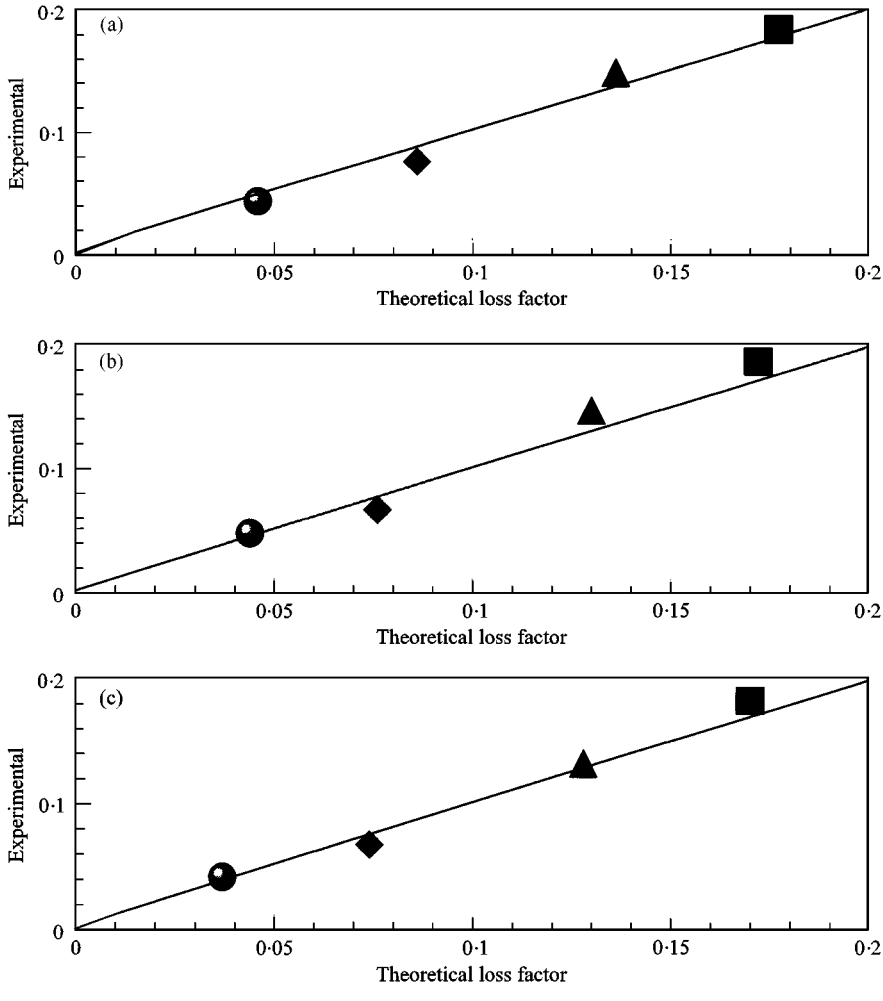

Figure 9. Comparison between theoretical and experimental loss factors of first bending mode for different k_p and k_d at (a) 25°C, (b) 35°C, (c) 45°C for full ACLD treatment (●, $k_p = 00$, $k_d = 00$; ◆, $k_p = 30$, $k_d = 50$; ▲, $k_p = 60$, $k_d = 130$; ■, $k_p = 120$, $k_d = 220$).

28·31 Hz. With 25 elements, the corresponding values converge to 4·48 and 27·58 Hz.

5. CONCLUSIONS

The theoretical predictions of a finite element model simulating the dynamics and control of plates treated with ACLD were compared with the experimental measurements. Experimental results were presented at three different operating temperatures (25, 35 and 45°C). It was found that activating the ACLD treatment has resulted in effective attenuation of the plate vibrations. It is observed also that

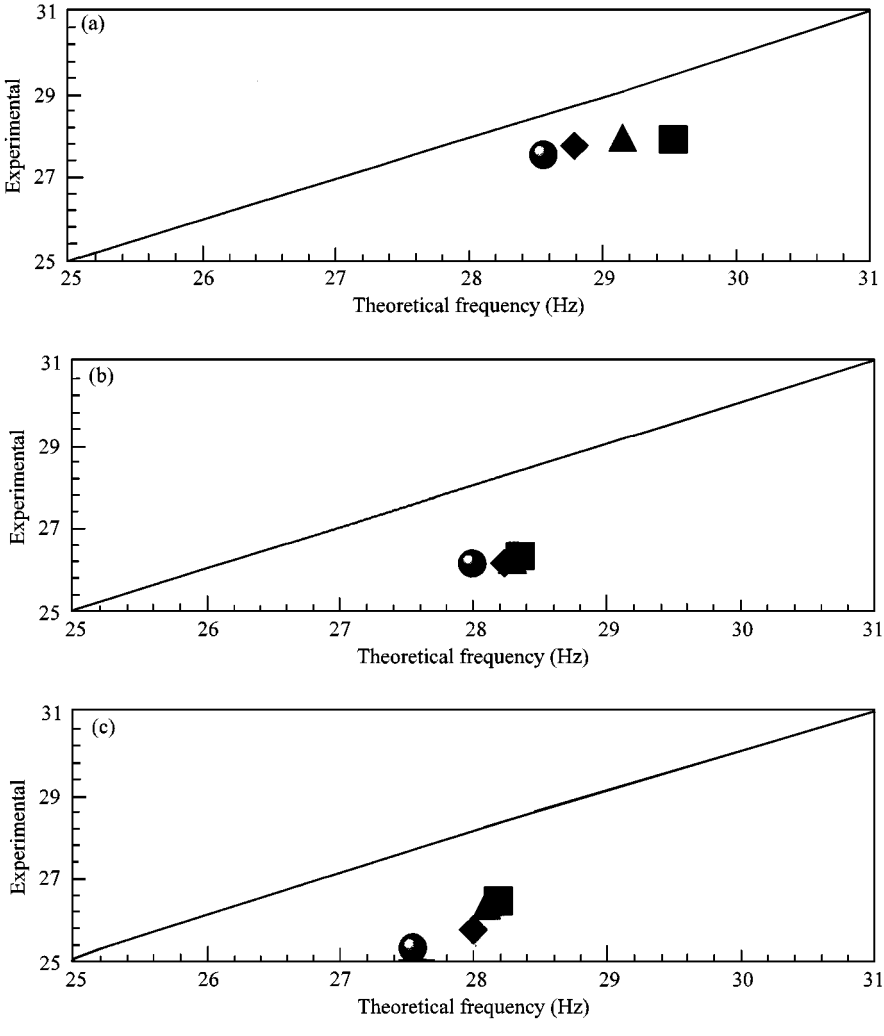

Figure 10. Comparison between theoretical and experimental natural frequencies of second bending mode for different k_p and k_d at (a) 25°C, (b) 35°C, (c) 45°C for full ACLD treatment (●, $k_p = 00$, $k_d = 00$; ◆, $k_p = 30$, $k_d = 50$; ▲, $k_p = 60$, $k_d = 130$; ■, $k_p = 120$, $k_d = 220$).

increasing the control gain has resulted in improving the vibration attenuation characteristics of the ACLD treatment. The theoretical and experimental modal frequencies and associated loss factors are compared for the first two bending modes. The results showed good agreement in the natural frequencies and loss factors evaluated by two methods. Hence, the developed theoretical and experimental techniques developed in this study constitute an invaluable tools for designing and predicting the performance of the smart laminated structures that could be used in many engineering applications.

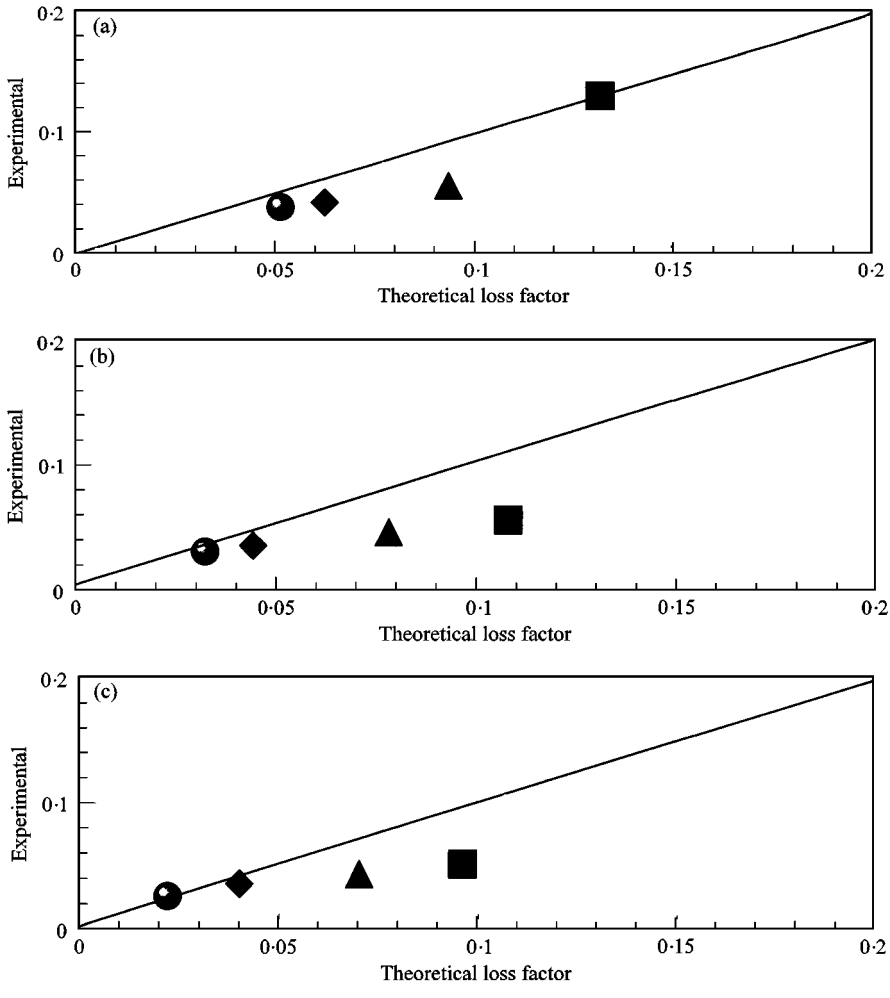

Figure 11. Comparison between theoretical and experimental loss factors of second bending mode for different k_p and k_d at (a) 25°C, (b) 35°C, (c) 45°C for full ACLD treatment (●, $k_p = 00$, $k_d = 00$; ◆, $k_p = 30$, $k_d = 50$; ▲, $k_p = 60$, $k_d = 130$; ■, $k_p = 120$, $k_d = 220$).

ACKNOWLEDGMENTS

This work is funded by the U.S. Army Research office (Grant number AASERT DAAH 04-94-G-0163). Special thanks are due to Dr Gary Anderson, the technical monitor, for his invaluable technical inputs.

APPENDIX A: STIFFNESS AND MASS MATRICES OF THE PLATE/ACLD SYSTEM

The strains can be divided into two parts, in-plane and bending. Presenting the strain–displacement matrix of each lamina, the in-plane and bending stiffnesses matrix $[K_i]$ of the ith element of the plate/ACLD system is obtained.

The stiffness matrix $[K_i]$ of the ith element of the plate/ACLD system is given by

$$[K_i] = \sum_{j=1}^{4} [K_{pj}] + [K_{s3}] + [K_{be}], \tag{A1}$$

where $[K_{pj}]$ denote the in-plane stiffness of jth layer respectively. The matrix $[K_{s3}]$ defines the shear stiffness matrix of the viscoelastic layer. Also $[K_{be}]$, is the bending stiffness matrix of plate/ACLD system. These stiffness matrices can be written as

$$[K_{pj}] = h_j \int_{ai} \int_{bi} [B_{jp}]^{\mathrm{T}} [D_{jp}] [B_{jp}] \, \mathrm{d}x \, \mathrm{d}y, \quad j = 1, \ldots, 4, \tag{A2}$$

$$[K_{s3}] = G_3 h_3 / 1{\cdot}2 \int_{ai} \int_{bi} [B_g]^{\mathrm{T}} [B_g] \, \mathrm{d}x \, \mathrm{d}y, \quad [K_{be}] = \int_{ai} \int_{bi} [B_b]^{\mathrm{T}} [D_b] [B_b] \, \mathrm{d}x \, \mathrm{d}y, \tag{A3, 4}$$

where G_3 denotes the shear modulus of the viscoelastic layer defined by $G'(I + \mathrm{i}\eta_3)$ and 1·2 in equation (A3) is the shear factor [10]. Also, the strain–displacement matrices $[B_{jp}]$, $[B_b]$ and $[B_g]$ are given by

$$[B_{jp}] = \begin{bmatrix} [N_{1,j}]_{,x} \\ [N_{2,j}]_{,y} \\ [N_{1,j}]_{,y} + [N_{2,j}]_{,x} \end{bmatrix}, \qquad [B_b] = \begin{bmatrix} -[N_3]_{,xx} \\ -[N_3]_{,yy} \\ -2[N_3]_{,xy} \end{bmatrix}$$

and

$$[B_g] = d/h_3 \begin{Bmatrix} ([N_{1,4}] - [N_{1,2}])/d + [N_{3,x}] \\ ([N_{2,4}] - [N_{2,2}])/d + [N_{3,y}] \end{Bmatrix}, \tag{A5}$$

The first subscript represents the shape function and the second represents the jth layer. The inplane stiffness $[D_{jp}]$ is given by

$$[D_{jp}] = \begin{bmatrix} D_{jp11} & D_{jp12} & 0 \\ D_{jp21} & D_{jp22} & 0 \\ 0 & 0 & D_{jp33} \end{bmatrix} \tag{A6}$$

with $D_{jp11} = D_{jp22} = E_j/(1 - v_j^2)$, $D_{jp12} = D_{jp21} = v_j E_j/(1 - v_j^2)$ and $D_{jp33} = E_j/[2(1 + v_j)]$ where E_j and v_j denote Young's modulus and the Poisson ratio of the jth layer respectively.

The equivalent bending stiffness $[D_b]$ of ACLD for plates can be written as

$$[D_b] = \sum_{j=1}^{4} [D_{bj}], \tag{A7}$$

where $[D_{b1}]$, $[D_{b2}]$, $[D_{b3}]$ and $[D_{b4}]$ are the flexural rigidity of the base plate, the sensor, the viscoelastic and the actuator layer respectively. These rigidities are

given by

$$[D_{bj}] = \left[\frac{E_j(t_{j+1}^3 - t_j^3)}{3(1 - v_j^2)}\right]\begin{bmatrix} 1 & v_j & 0 \\ v_j & 1 & 0 \\ 0 & 0 & \frac{1}{2}(1 - v_j) \end{bmatrix}, \tag{A8}$$

where E_j and v_j denote Young's modulus and the Poisson ratio of the jth layer respectively.

The mass matrix $[M_i]$ of the ith element of the plate/ACLD system is given by

$$[M_i] = \sum_{j=1}^{4} [M_{bj}] + \sum_{j=1}^{4} [M_{pj}], \tag{A9}$$

where $[M_{bj}]$ and $[M_{pj}]$ denote the mass matrices due to bending and extension of the jth layer respectively. These mass matrices can be written by

$$[M_{bj}] = \rho_j h_j \left[\int_{ai}\int_{bi} ([N_3]^{\mathrm{T}}[N_3])\,\mathrm{d}x\,\mathrm{d}y\right] \tag{A10}$$

and

$$[M_{pj}] = \rho_j h_j \left[\int_{ai}\int_{bi} ([N_{1,j}]^{\mathrm{T}}[N_{1,j}] + [N_{2,j}]^{\mathrm{T}}[N_{2,j}])\,\mathrm{d}x\,\mathrm{d}y\right], \tag{A11}$$

where ρ_j and h_j represent the density and thickness of the jth layer respectively.

REFERENCES

1. H. Ghoneim 1993 *SPIE Proceedings*: *Mathematics in Smart Structures*, **1919**, 78–98. Electromechanical surface damping using constrained layer and shunted piezoelectric.
2. I. Y. Shen 1994 *Journal of Smart Materials and Structures* **3**, 59–70. Bending vibration control of composite and isotropic plates through intelligent constrained layer treatments.
3. A. Baz 1996 *U.S. Patent*, #5, 485, 053. Active constrained layer damping.
4. T. P. Khatua and Y. K. Cheung 1973 *International Journal for Numerical Methods in Engineering* **6**, 11–24. Bending and vibration of multilayer sandwich beams and plates.
5. D. H. Robbins and J. N. Reddy 1993 *International Journal for Numerical Methods in Engineering* **36**, 655–677. Modeling of thick composites using a layerwise laminate theory.
6. J. N. Reddy 1997 *Mechanics of Laminated Plates*: *Theory and Analysis*. Boca Raton, FL: *CRC* Press.
7. R. D. Cook, D. S. Malkus and M. E. Plesha 1989 *Concepts and Applications of Finite Element Analysis*, third edition. 314–322. New York: Wiley.
8. IEEE Std 176-1987 *IEEE Standard on Piezoelectricity*, 1987 The Institute of Electrical and Electronic Engineers, 9–15.
9. E. Crawley and K. B. Lazarus 1991 *American Institute of Aeronautics and Astronautics Journal* **29**, 944–951. Induced strain actuation of isotropic and anisotropic plates.
10. K. H. Ha 1990 *Computers and Structures* **37**, 397–403. Finite element analysis of sandwich plates: an overview.